SAND21XX-XXXXR
LDRD PROJECT NUMBER: 227032
LDRD PROJECT TITLE: Developing a high-speed terahertz imaging system based on parametric upconversion imaging for penetrative sensing
PROJECT TEAM MEMBERS: Lyle Pickett (PI), Logan White, Julien Manin

ABSTRACT

Imaging using THz waves has been a promising option for penetrative measurements in environments that are opaque to visible wavelengths. However, available THz imaging systems have been limited to relatively low frame rates and cannot be applied to study fast dynamics. This work explores the use of upconversion imaging techniques based on nonlinear optics to enable wavelength-flexible high frame rate THz imaging. UpConversion Imaging (UCI) uses nonlinear conversion techniques to shift the THz wavelengths carrying a target image to shorter visible or near-IR wavelengths that can be detected by available high-speed cameras. This report describes the analysis methodology used to design a prototype high-rate THz UCI system and gives a detailed explanations of the design choices that were made. The design uses a high-rate pulse-burst laser system to pump both THz generation and THz upconversion detection, allowing for scaling to acquisition rates in excess of 10 kHz. The design of the prototype system described in this report has been completed and all necessary materials have been procured. Assembly and characterization testing is on-going at the submission of this report. This report proposes future directions for work on high-rate THz UCI and potential applications of future systems.

Sandia National Laboratories is a multimission laboratory managed and operated by National Technology and Engineering Solutions of Sandia, LLC, a wholly owned subsidiary of Honeywell International, Inc., for the U.S.

Department of Energy's National Nuclear Security Administration under contract DE-NA-0003525.

INTRODUCTION

This report describes the approach and results from a one-year, late-start LDRD project to investigate the feasibility of a high-speed THz imaging system. Specifically, this study focuses on UpConversion Imaging (UCI) for THz imaging in a system that can be scaled to high frame rates. The main aim of this study is to develop a prototype high-speed THz UCI system that can be used to evaluate the efficacy of the high-speed UCI strategy. As a note for clarity, all frequencies provided in THz units correspond to electromagnetic frequencies while values in kHz or MHz refer to acquisition rates.

Since the start of the 21st century, there have been significant improvements in THz wave detection technologies that have led to a rapid expansion of THz-based measurement applications. A key feature of THz waves (defined here as electromagnetic waves with wavelengths between 30 to 600 μm, corresponding to electromagnetic frequencies between 0.5 to 10 THz – $\lambda = c/\nu$) is that their long wavelengths penetrate through many materials that are opaque at visible and IR wavelengths. This penetrating capability has been leveraged in THz imaging techniques for many applications of penetrative sensing [1], including inspection of structural foams [2], inspection of foods [3], and composite fiber orientation sensing [4]. These are in addition to various biomedical [5] and chemistry applications [6].

In addition to low-speed applications where THz imaging has been previously explored, there are problems of interest with high-speed dynamics where penetrative THz imaging could be beneficial. These areas of interest to the laboratories include atomized sprays for industrial and energy systems where light scattering creates excessive light extinction at visible wavelengths [7]. Liquid fuel sprays for advanced engines and propulsion systems evolve on sub-millisecond time scales and require imaging rates over 10,000 frames per second to resolve important dynamics [8]. THz imaging in these environments could enable quantitative descriptions of liquid spray dynamics in the spray regions that are inaccessible with current techniques. Studies of explosions apply extremely high rate imaging (≥1 million frames per second) [9] that can be limited by dense smoke and dust. High-rate THz imaging in explosions may allow observation of wave structures and thermochemical dynamics within the smoke cloud.

The expansion of THz imaging to these and other dynamic environments has been prevented by the lack of available high-speed THz imaging technologies and techniques. Many scientific applications of THz imaging use raster scanning of pointwise THz detection techniques, such as THz time-domain spectroscopy [10], which offer precise but slow measurements. Commercially available array detectors capable of rapid image acquisition are based on two technologies: micro-bolometers and THz-sensitive semiconductors. Micro-bolometers are miniaturized thermal-based detector arrays that exhibit high-sensitivity but are limited to lower frame rates

[11]. Semiconductor array THz imagers are available in sensor formats of up to 2048×2048 (DataRay Inc. WinCamD-THz [12]) but are typically limited to acquisition rates of 60 frames per second or less. Due to their low speed, commercially available THz systems are not capable of high-rate THz imaging.

The only example of high-speed THz imaging in published work is the atomic vapor technique described by Downes et al. [13] The technique used atomic cesium vapor excited by laser pumping into an upper Rydberg state where absorption of THz photons caused a transition to a neighboring fluorescent Rydberg state. Imaging of visible fluorescence from the vapor could then be used to detect the image initially carried by the THz photons. The technique was demonstrated up to an acquisition rate of up to 3 kHz. However, as the authors point out, the technique's speed is only physically limited by the 0.8 microsecond lifetime of the excited cesium state, which means that it could be scaled to MHz frame rates. The major drawback of this technique is the restriction of the detectable THz frequencies to the transition of the atomic vapor, 0.55 THz in this case. Practical high-rate imaging for multiple applications will prefer or require an alternative high-rate imaging technique with more wavelength versatility. The approach we propose in this work, also mentioned by Downes et al. [13], is to use UCI for rapid THz imaging.

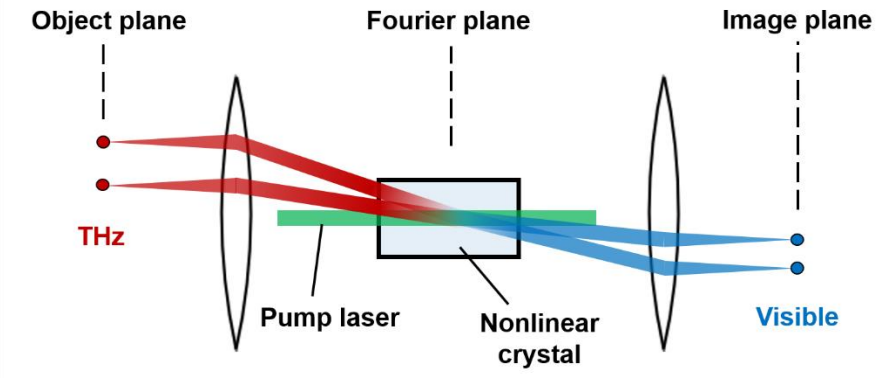

Figure 1 – A conceptual schematic of the UCI approach where a nonlinear crystal hosts an SFG process at the Fourier plane of a 4f imaging configuration. The system takes THz waves emitted from the object plane and transforms them into a visible image on a sensor at the image plane.

UCI is a technique that leverages parametric frequency conversion processes in a nonlinear medium to convert the wavelength of light carrying a target image from long, undetectable wavelengths to shorter wavelengths that can be readily detected with available cameras. This work considers UCI designs based on Sum-Frequency Generation (SFG) processes hosted in nonlinear crystals and pumped with high-rate pulsed lasers. The crystal and incident laser pump beam act as an aperture in the imaging system, which is arranged as a 4f imaging configuration with the crystal placed at its Fourier plane (common focus plane). Therefore, the SFG process

controls the spatial, temporal, spectral, and polarization response of the imaging system, making the choice of SFG parameters critical in system design. The important advantage of the UCI approach is its fast temporal response, as the pulse duration and repetition rate of the pump laser determine the system's exposure time and frame rate, respectively. Therefore, combining modern pulse-burst laser systems with high-speed CMOS cameras can enable high-speed THz imaging through UCI.

The feasibility of THz UCI has been demonstrated by prior experimental work. Tekavec et al. [14] used a novel THz generation scheme to perform active imaging with a THz UCI system. Fan et al. [15] demonstrated diffraction-limited THz imaging using a video-rate UCI system. Pfieffer et al. [16] performed a spectrally-resolved characterization of a THz UCI sytem, confirming models of expected UCI response. While these examples demonstrate the feasibility of UCI-based THz imaging, none of them demonstrated the high frame-rates sought in this project. The highest frame-rate achieved was 100 frames per second by Fan and co-workers. This work is focused on realizing the high-speed potential of this proven approach to THz imaging.

The aim of the system design in this work is to leverage available capital equipment to create a proof-of-concept prototype high-speed THz UCI system that can be used to evaluate the feasibility of the high-speed UCI approach. A high-speed pulse-burst laser system is available for this effort that can operate at repetition rates in excess of 100 kHz with ns-scale pulse durations (approximately 12 ns) provided by Nd:YAG amplification (1064 nm fundamental wavelength and a 532 nm wavelength second harmonic). This can be used to pump the high-speed UCI process, as well as potential high-speed THz sources (discussed below). High frame rate silicon CMOS cameras are also available for detection of the upconverted image signals. The system-level design of the THz UCI prototype comprises determining optimal SFG parameters and appropriate optical components. One aspect of this design is the choice of THz source for active imaging measurements.

Because there are few strong THz emitters in nature and applications of interest rarely provide nascent THz illumination, THz imaging systems are typically active imaging systems that include an intense THz source to illuminate the scene. The choice of THz source is critical to the capabilities and performance of an imaging system, and the application of UCI imposes additional constraints on the choice of THz source. Prior THz UCI systems have used PhotoConductive Antennae (PCAs) [16] and Difference-Frequency Generation (DFG) with nearly degenerate Optical Parametric Oscillators (OPOs) [14, 15] to generate pulsed THz radiation. These options have several drawbacks that make them impractical for use in a high-speed system driven by a ns-pulsed Nd:YAG pulse-burst laser system, as intended for this design. Instead, a THz Parametric Generator (TPG) design [17] based on an orthogonal QPM design [18] was investigated in this work. This approach offers high-energy, narrowband THz

pulse generation with ns-pulsed laser pumping that can be practically scaled to high repetition rates.

This report documents the design and preliminary testing of a prototype high-speed THz UCI system that can be used to evaluate the feasibility of such an approach. The next section of the report, the methodology section, describes the requisite theory and analysis tools needed to perform a design analysis for a THz UCI system. The results and discussion section describes the detailed design of the high-speed THz UCI prototype system and proposes tests of its performance. The anticipated outcomes and impacts section provides recommended next steps to advance this work toward a system with improved imaging resolution that might be applied to problems of interest.

DETAILED DESCRIPTION OF RESEARCH AND DEVELOPMENT AND METHODOLOGY

This section describes the modeling and design methodology necessary to construct a UCI-based THz imaging system. A large portion of this description focuses on the details of the SFG process and how to model the dependence of conversion efficiency on relevant parameters. The analysis also addresses other aspects of UCI, such as the selection of imaging optics and target THz frequencies. The end of this section explores the requirements and candidates for THz sources for illumination of active imaging.

THz UCI detection

Understanding and modeling the SFG process is critical to designing a UCI system. This is because the UCI process determines what light is and is not detected by the UCI measurements. Any long wavelength light that SFG does not efficiently convert will be invisible to the sensor at the imaging plane of the system. Through the position of the nonlinear crystal at the Fourier plane of the imaging system, the SFG process controls the system's spectral, temporal, and spatial response by acting like a fast aperture. In the case of most UCI systems, including the one described in this work, the SFG process is also polarization selective. Therefore, by tailoring the design of the SFG process, the desired acceptance and rejection properties can be achieved to suit a particular application.

The SFG process is a second-order nonlinear process that can be modeled using the theory of nonlinear optics. Under a few approximations generally appropriate for SFG in UCI systems, expressions can be derived that predict SFG conversion efficiency and how it varies with several parameters. Perhaps the most critical parameters are the wavelengths of the fields that participate in the SFG process. For a given pair of THz and pump wavelengths, the law of conservation of energy uniquely determines the upconverted signal wavelength. This is captured in the

relationship between wavelengths, λ, shown in Eq. (1) where the subscripts THz, pump, and UC represent the THz field, pump field, and upconverted field, respectively.

$$\lambda_{\mathrm{UC}}^{-1} = \lambda_{\mathrm{pump}}^{-1} + \lambda_{\mathrm{THz}}^{-1} \quad (1)$$

While all THz wavelengths are uniquely mapped to output wavelengths, only specific THz wavelengths are efficiently converted by the system. Which wavelengths are converted and therefore detected are determined by the phase-matching criterion.

The phase-matching criterion is the requirement that the nonlinear polarization wave generated by the interaction of the input waves within the nonlinear crystal must propagate in phase with the output wave of the SFG process. This condition can be expressed mathematically by requiring that the sum of the wavevectors of the input waves is equal to the sum of the wavevectors of the output waves, as shown in Eq. (2).

$$\Delta\vec{k} = \vec{k}_{\mathrm{THz}} + \vec{k}_{\mathrm{pump}} - \vec{k}_{\mathrm{UC}} = 0 \quad (2)$$

Here, the wavevector of the i$^{\mathrm{th}}$ field is $k_i = 2\pi n_i/\lambda_i$, where n_i is the refractive index in the crystal at that wavelength and λ_i is the wavelength of that field. An alternative interpretation of this relationship is that it is a conservation of photon momentum condition within the nonlinear crystal. When this condition is satisfied, power will flow into the output field of the SFG process to produce exponential growth along the length of the crystal.

While perfect phase-matching can sometimes be achieved for a target wavelength with a desired combination of pump laser and nonlinear crystal, it is often not easily satisfied. One approach is to compromise the choice of pump laser and nonlinear crystal material until phase-matching is satisfied; however, this may not be possible or acceptable for some applications. An attractive alternative is an approach known as Quasi-Phase Matching (QPM). In QPM, the directional properties of the nonlinear crystal are periodically reversed along a particular direction within the crystal (often the direction of light propagation within the crystal). The spatial interval over which the directional properties are reversed and reversed back is known as the poling period, Λ_{p}. The poling period can be chosen to precisely cancel the phase mismatch accumulating in the SFG process by satisfying the QPM criterion shown in Eq. (3).

$$\Delta k_{\mathrm{QPM}} = k_{\mathrm{THz}} + k_{\mathrm{pump}} - k_{\mathrm{UC}} \pm \frac{2\pi}{\Lambda_{\mathrm{p}}} = 0 \quad (3)$$

In that case, efficient SFG conversion is achieved for the target wavelength with an efficiency penalty factor of $(2/\pi)^2 \approx 0.4$ relative to perfect phase-matching.

Importantly, QPM gives a designer control over the wavelengths that are converted by the system through the selection of the poling period. Nonlinear crystals can be designed with multiple poling periods side-by-side so that spectral response bands can be quickly changed with small translations of the crystal. Crystals can also be designed with fan-out poling to enable spectral tuning through rotation of the crystal [19] or with chirped poling periods to increase the

bandwidth of the system's spectral response [20]. QPM designs can be conveniently realized in some nonlinear crystal materials, such as Lithium Niobate (LN), through a manufacturing process called periodic poling [21]. QPM can be similarly implemented in optical semiconductor materials like GaP through a crystal growth process called Optical-Patterning (OP) [22]. In principle, any nonlinear crystal can be used in QPM by optically-bonding slabs of alternating crystal orientations. However, this is often too difficult to control to generate crystals of desired lengths.

In addition to phase-matching, other considerations affect the efficiency of the SFG process, with the primary influences being nonlinear crystal material, crystal dimensions, and pump beam intensity. Depending on assumptions made, the overall SFG efficiency can be modeled in several ways [23]. However, in the weak, non-depleting pump approximation relevant to this work, the SFG efficiency, η, can be written as shown in Eq. (4) where d_{eff} is the effective nonlinear coefficient of the crystal medium (including QPM scaling described above), L is the length of the crystal, I_{pump} is the intensity of the pump beam, and n_i is the refractive index of the i^{th} field.

$$\eta = \frac{8\pi^2 d_{\text{eff}}^2 L^2 I_{\text{pump}}}{\varepsilon_0 n_{\text{THz}} n_{\text{pump}} n_{\text{UC}} c \lambda_{\text{THz}} \lambda_{\text{UC}}} \tag{4}$$

Note that the efficiency is inversely proportional to λ_{THz}. In mid-IR UCI, it is possible to apply pump laser intensities that reach unity conversion efficiency theoretically (determined using the strong pumping relationship, see Table 4 in [23]). However, for THz UCI, the extremely long wavelength drives optimal laser intensities above 1 GW/cm^2, well above the damage threshold for any nonlinear crystal material. This limits THz UCI to relatively low conversion efficiencies, making it more practical for active THz imaging measurements where the scene is illuminated with a strong source.

Another important factor influencing conversion efficiency is THz absorption within the nonlinear crystal hosting the SFG process. While mid-IR UCI can be performed using crystals with negligible absorption of the target wavelength, very few materials are highly THz transparent, and all known nonlinear crystal materials exhibit measurable THz absorption. The SFG efficiency relationship in Eq. (4) neglects THz absorption. However, it can be adjusted to account for absorption, as shown in Eq. (5) where α_{THz} is the THz absorption coefficient of the nonlinear crystal.

$$\eta = \eta_0 \exp\left(-\frac{\alpha_{\text{THz}} L}{2}\right) \frac{\sinh^2(\alpha_{\text{THz}} L/4)}{(\alpha_{\text{THz}} L/4)^2} \tag{5}$$

Figure 2 shows the efficiency scaling factor resulting from absorption as a function of crystal length for several values of α_{THz} (LN, the medium chosen for the system in this work, has a value of $\alpha_{\text{THz}} = 2.7$ mm^{-1} at 1.5 THz). THz absorption is important to consider when designing the SFG crystal, as increasing absorption negates the efficiency improvements typically expected from increasing crystal length.

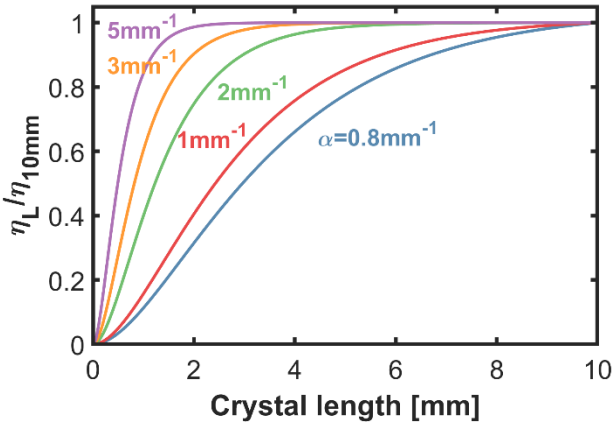

Figure 2 – The effect of THz absorption within the nonlinear crystal on conversion efficiency for various THz absorption coefficients. The absorption effect is plotted as the efficiency of a crystal of a particular length compared to the efficiency of a similar crystal that is 10 mm in length. This shows the diminishing returns caused by absorption.

The description of phase-matching given above implicitly assumes collinear propagation of all waves participating in the SFG process (as well as the crystal poling period vector in the case of QPM). In general, the phase-matching condition is a vectorial relationship that can be satisfied in three-dimensional space by non-collinear waves. This is necessary for imaging to be possible in the 4f UCI configuration adopted here, as different positions in the object plane map to different propagation directions within the nonlinear crystal at the Fourier plane. Figure 3 provides a notional (not to scale) representation of the non-collinear QPM process. Importantly, for a pump beam oriented along the system's optical axis, the off-axis component of the THz wavevector is exactly maintained as the off-axis component of the upconverted signal wavevector. This is how the upconversion process maintains spatial information in an image. Non-collinear phase-matching has several other implications that are important to understand during UCI system design.

For one, the fact that the off-axis components of the THz and upconverted wavevectors are the same combined with the much larger magnitude of the upconverted wavevector implies that the upconverted wave will propagate at a smaller angle relative to the optical axis. This relationship between the propagation angles of the THz and upconverted waves is given in Eq. (6).

$$\theta_{\mathrm{UC}} = \sin^{-1}\left[\frac{k_{\mathrm{THz}}}{k_{\mathrm{UC}}}\sin(\theta_{\mathrm{THz}})\right] \qquad (6)$$

The optical Fourier transform performed by the image-forming lens converts this angular contraction into an effective de-magnification of the image relative to the object size carried by the THz wave. This upconversion-induced de-magnification is proportional to the ratio of the THz and upconverted wavelengths: $\lambda_{\mathrm{UC}}/\lambda_{\mathrm{THz}} << 1$. De-magnification presents a major challenge

in the case of THz UCI because the wavelength ratio is large, almost three orders of magnitude. Because the energy of THz photons is so small, the pump and upconverted wavelengths are almost equal: $\lambda_{UC} \approx \lambda_{pump}$. This provides motivation for choosing the longest possible pump wavelength to mitigate de-magnification.

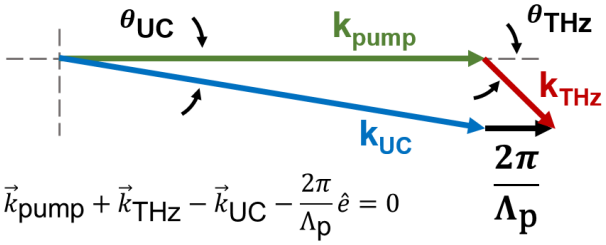

Figure 3 – A schematic showing the non-collinear QPM condition and the relationship between the propagation angles of the THz and upconverted fields. Note that the magnitudes of the wavevectors are not to scale as the pump and upconverted wavevectors are significantly larger than the THz wavevector.

The consequences of non-collinear phase-matching for the spatial dependence of a UCI system's spectral response can be visualized using what can be called a "THz tuning curve." An example of a THz tuning curve is shown in Figure 4. These curves plot contours of SFG efficiency as a function of THz wave propagation angle within the crystal on the horizontal axis and THz frequency on the vertical axis. These plots show the spectral response of a particular UCI system and how it varies with propagation angle, which can be directly related to position within the image. In mid-IR UCI systems, this spatial-spectral coupling of the SFG efficiency can lead to significant variation in the spectral response of the system across the field of view [24, 25]. In contrast, for THz systems, the low magnitude of the THz wavevector leads to less spatial dependence in the spectral response. Figure 5 shows this difference in spatial-spectral coupling with an example mid-IR tuning curve that exhibits significantly more non-collinearity effects than the example THz tuning curve in Figure 4. THz tuning curves are an important tool for evaluating UCI system designs.

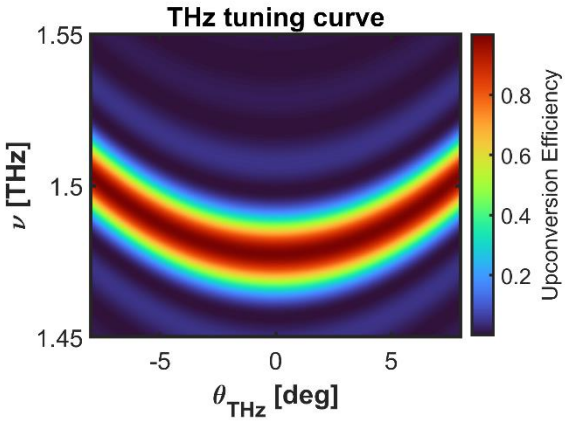

Figure 4 – Example THz tuning curve for a relevant THz UCI system. The horizontal axis represents propagation angle within the crystal, but can be thought of as position in the image. Color contours show conversion efficiency.

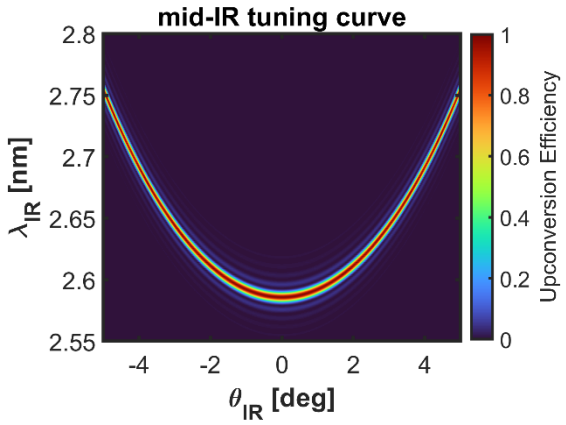

Figure 5 – Example of a tuning curve for a mid-IR UCI system for comparison with the THz tuning curve. The thin, steeply curving shape of the efficient region is indicative of strong spatial-spectral coupling that is not present in THz UCI.

So far, spatial image information has been discussed as an angular separation from the optical axis. The properties of the lenses in the 4f imaging configuration, specifically their effective focal lengths, determine the relationship between propagation angle in the Fourier plane and spatial locations in the object and image planes. By trigonometry, these relationships are $r_{\mathrm{Ob}} \approx n_{\mathrm{THz}} f_{\mathrm{Ob}} \theta_{\mathrm{THz}}$ and $r_{\mathrm{Im}} \approx n_{\mathrm{UC}} f_{\mathrm{Im}} \theta_{\mathrm{UC}}$ in the small θ_{THz} limit. Therefore, optics should be chosen so that the desired field of view fits within the angular acceptance determined by the THz tuning curve and the image fits on the detector area. The choice of lenses also affects the achievable image quality, as the Gaussian width of the Point Spread Function (PSF) of a UCI system can be expressed as shown in Eq. (7) [26] where w_0 is the beam waist of the pump beam.

$$\Delta_{\mathrm{PSF}} = \frac{\sqrt{2\ln(2)}\,\lambda_{\mathrm{UC}} f_{\mathrm{Im}}}{\pi w_0} \tag{7}$$

An important decision in UCI system design is the selection of the pump wavelength for the SFG process. As described above, the pump wavelength determines the magnitude of upconversion de-magnification experienced by the UCI system. Shorter pump wavelengths lead to greater de-magnification, which is especially significant for THz UCI and may be a limiting factor in image quality. However, this decision is also affected by the choice of the nonlinear crystal for upconversion, as some crystals strongly absorb bands of pump wavelengths. For example, organic crystals like DAST and OH1 only transmit wavelengths above 700 nm [27]. In this way, the choice of nonlinear crystal and SFG pump wavelength should be co-optimized. In this work,

the need to base the system design around pumping with an Nd:YAG laser source limits the choice of available pump wavelengths to the fundamental 1064 nm field and its harmonics: 532 nm, 355 nm, and 266 nm. Because of the severity of the de-magnification and the weak camera response at UV wavelengths, only 1064 nm and 532 nm are considered pump wavelength candidates in this work.

As discussed in the introduction, a key feature of the UCI approach to THz imaging is enabling wavelength flexibility in a high-speed detection system. The UCI technique pursued here provides some on-the-fly tuning of the system's wavelength response. By changing the temperature of the upconversion crystal, the refractive index changes (and to a lesser extent, the poling period changes due to thermal growth), which leads to a different QPM condition. Due to the low wavevector magnitudes of the THz waves, temperature tuning exhibits a much smaller range than can be realized at mid-IR wavelengths. A more effective way to augment the spectral response of the UCI system is by using different poling periods to center the response at different THz frequencies. For some crystal media, this may require the fabrication of multiple crystals. In the case of LN, periodically-poled Lithium Niobate (ppLN) crystal chips can be manufactured with multiple poling periods placed side-by-side on the same chip. For systems using these crystal chips, the wavelength response can be changed by translating the chip laterally a few millimeters while maintaining its position in the optical arrangement. This provides an avenue for quick wavelength tuning.

The selection of THz wave frequencies to target with an imaging system is important because of strong absorption by water molecules. Unless the atmosphere of a test apparatus is purged or dehumidified, strong H_2O transition lines can limit the propagation length of some THz frequencies to less than a meter. Therefore, it is advisable to choose THz wavelengths away from strong H_2O transition frequencies and target what are called "water windows" in the THz spectrum. Figure 6 shows THz atmospheric transmission data reported by Yang et al. [28]. These data provide several examples of water windows that might be targeted, including 0.68, 0.85, and 1.49 THz. When choosing THz frequencies to target, one should consider that the diffraction limit for spatial resolution is inversely proportional to wave frequency. This means that imaging resolution can change by more than a factor of two over this range of water windows. This resolution effect can be significant for THz imaging since minimum resolvable sizes are generally greater than 100 μm and make imaging small features challenging.

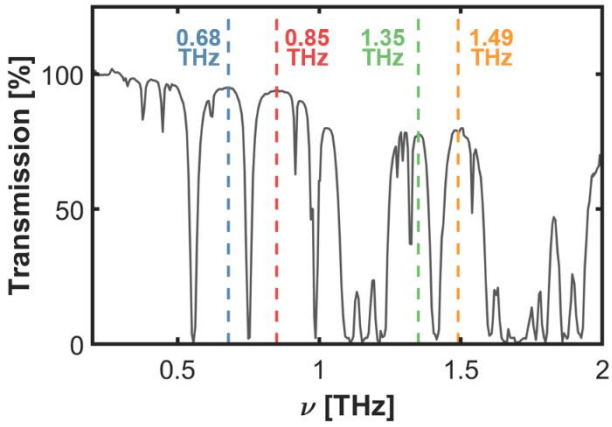

Figure 6 – Atmospheric THz transmission spectrum with water windows that were targeted in prototype system design. Transmission data is from Yang et al. [28]

THz generation

As described above, THz UCI systems exhibit a limited detection efficiency that generally requires strong THz sources for active imaging. An appropriate source must provide intense THz radiation that meets several requirements driven by the specifics of UCI. These include the need for the THz light to overlap in time and wavelength with the response of the UCI system, as well as the need for it to be polarized since only one polarization component will participate in the SFG process. The specific goal of this project is to develop a prototype high-speed UCI system that is compatible with available laser systems. It is then desirable to choose a THz generation technique that can be pumped with an Nd:YAG laser.

Several THz generation strategies typically used for THz imaging studies include PhotoConductive Antennae (PCAs) [29], Optical Rectification [30], and Difference Frequency Generation (DFG) of nearly-degenerate OPO output [31]. While effective in some applications, these approaches to THz generation have some significant drawbacks for this high-speed UCI system. For one, PCAs and OR tend to generate relatively broadband THz radiation. This is sub-optimal for the UCI system because the QPM condition is expected to generate a narrowband THz spectral acceptance. Therefore, the THz source should be chosen to generate narrowband THz output that highly overlaps with the UCI system's response. DFG-based techniques typically generate tunable narrowband THz radiation that is compatible with UCI, as demonstrated by Fan et al. [15] and Tekavec et al. [14] However, these approaches are often more complicated to design and operate, more expensive to implement, and require a larger spatial footprint.

Another important restriction of some of these techniques is the need for fs-pulsed pumping. While DFG does not require fs-pulsed laser pumping, PCAs and OR generally require these short pulses and are not compatible with ns-pulsed pumping. While a THz UCI system could be operated with an independent THz generation pump laser, the reduction in complexity and cost associated with using a single laser system to pump both the THz source and UCI detection is attractive. The pulse-burst Nd:YAG system considered in this work exhibits a pulse duration of approximately 10 ns. The possibility of achieving single-laser THz generation and UCI detection motivates the exploration of THz generation approaches compatible with that pulse duration.

One promising family of THz generation techniques compatible with ns-pulsed pumping is TPG and THz OPO (TPO) in LN crystals. There are several specific approaches within this family, including unseeded TPO [32], seeded TPO [33], unseeded TPG [34], seeded TPG [35, 17], and non-axial QPM [18, 36]. These techniques have been demonstrated to produce up to nJ level pulse energies, significant spectral tunability, and repetition rate scaling up to kHz rates. The techniques produce fairly narrowband THz radiation, and the bandwidth can be further narrowed using signal wavelength seeding. Challenges can include the need for precise spatial alignment of the beams, high THz absorption in LN, and a high pulse energy threshold for generation.

The TPO and TPG processes decompose incoming energy at the pump wavelength into two fields of longer wavelengths. By convention, the shorter of the two output wavelengths is called the "signal" field, while the longer wavelength is called the "idler" field. In the case of the THz generation, the idler wavelength is that of the THz frequency being generated, and the signal wavelength is determined by the difference in pump and idler wavelengths (for example, a 1064 nm pump field producing 1.5 THz radiation will have a signal wavelength of 1070 nm). The efficiency and bandwidth of these processes can be augmented by seeding the signal field with a low-power beam. Kawase et al. [35] showed that seeding improved TPG efficiency and output threshold, while Walsh et al. [33] showed a significant narrowing of TPO output through seeding. Given these benefits, it is important to consider what impact seeding can have on TPO and TPG strategies.

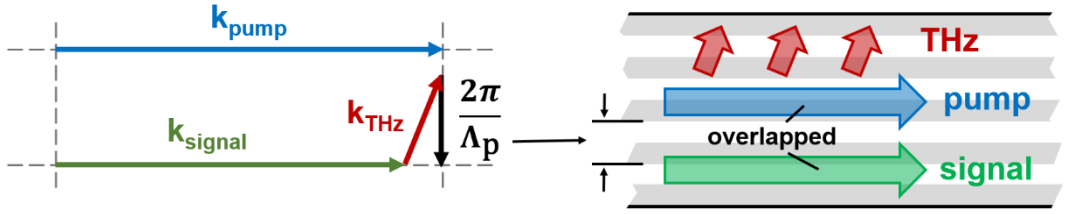

Figure 7 – A schematic illustrating the "sideways" poled TPG process with the QPM condition shown on the left and propagation of the participating fields within the crystal on the right.

As discussed above in the context of SFG for UCI detection, nonlinear processes that fail to satisfy perfect phase-matching can be enhanced through a QPM process. QPM can be similarly applied to enable THz generation interactions that would otherwise not be possible. Molter et al. [18] proposed a novel TPO technique based on non-collinear QPM where the poling period is oriented at 90 degrees relative to the propagation direction of the pump beam. The upshot of this approach is that pump and signal beams can experience strong, collinear interaction along the entire length of the crystal. This is expected to improve conversion efficiency and overall THz energy generation compared to other mixing schemes where the pump and signal beams propagate in different directions. In this arrangement, the THz radiation is generated to propagate at an angle relative to the pump beam's direction of propagation. The THz radiation is then output through one of the side facets of the crystal. An added benefit of this approach is that the sideways propagation of the THz waves toward an adjacent facet of the crystal reduces the THz path length within the crystal and mitigates associated THz absorption by LN.

RESULTS AND DISCUSSION

As of the submission of this report, the design activities and procurement of necessary equipment to assemble and test the prototype high-speed THz UCI system have been completed. Assembly and alignment of the THz generation system have been completed and it is ready for testing. In continuing work after this late-start project, the UCI detection module described below can be assembled and tested using the output from the THz generation system. This section focuses on a detailed description of the system design that resulted from the efforts of this project and proposes a testing regime that can capture the data needed to draw conclusions about the practicality of high-speed THz UCI.

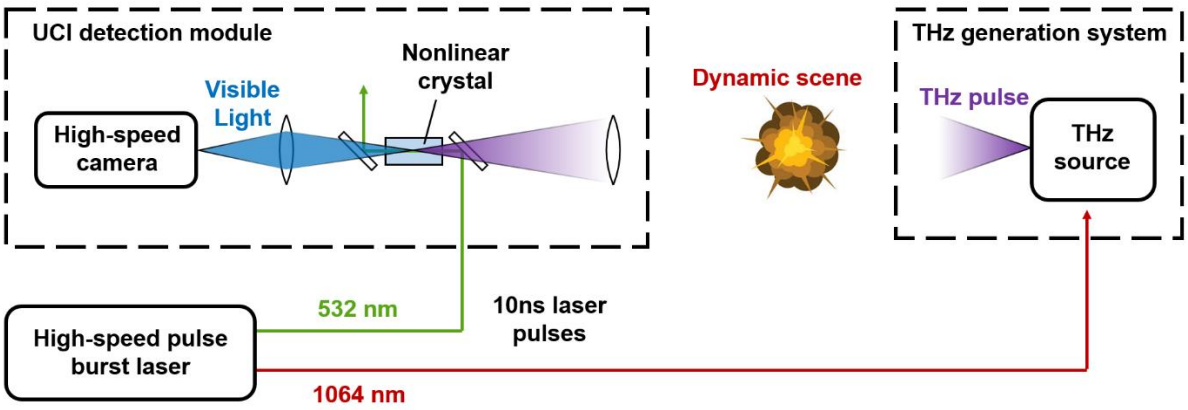

Figure 8 – A schematic showing the major components of a high-rate THz UCI system. Here, the decomposition into THz generation and UCI detection module sub-systems is highlighted.

This work describes the design and procedure for testing a complete high-speed THz UCI system, including the THz source and UCI detection module. However, for design purposes, it is convenient and intuitive to treat the overall system as a composite of two sub-systems: the THz generation system and the UCI detection module. The design and proposed testing for each of these sub-systems are described separately in this section.

THz generation design: TPG based on sideways QPM

As discussed in the prior section, a "sideways" QPM strategy provides an opportunity for high pump-signal overlap and efficient THz generation at a target frequency. The technique has been demonstrated to be effective for THz generation with the ns-pulsed, 1064 nm pump beams [18] provided by the pulse-burst laser considered in this work. Unlike prior implementations of this sideways QPM technique, this work uses a single-pass TPG design rather than a cavity-enhanced TPO design. One reason for this change is that the high pulse energies offered by the pulse-burst laser (>100 mJ/pulse) are sufficient to pump high-energy THz generation without the need for cavity enhancement. Additionally, the nearly degenerate relationship between the pump beam at 1064 nm and the signal beam at 1070 nm makes it difficult to design appropriate cavity mirrors for collinear TPO. The switch to a TPG configuration will also be less susceptible to Raman lasing that had been observed to resonate in the TPO cavity.

The TPG approach was implemented using a ppLN crystal chip with the same dimensions as that of Molter et al. [18]: 50 mm × 3 mm × 1 mm. The crystal is fabricated with a 44 μm poling period oriented orthogonal to the direction of light propagation. Because of the collinear propagation of the pump and signal beams, THz radiation can be generated along the entire 50 mm path length of the crystal. The 1 mm aperture was chosen to limit costs associated with crystal fabrication. The combination of a long crystal path length and small aperture makes the optical alignment of the pump beam, seeding beam (described below), and the crystal axis challenging. The output of the TPG process will be roughly collimated with a 75 mm focal length PTFE plano-convex lens. More sophisticated collimation approaches have been used in other works and might be explored for future applications.

A custom chip holder is required to effectively integrate the custom ppLN crystal into the THz generation system. The ppLN chip for this system was designed to operate at room temperature without the need for active heating, which is required in the UCI chip holder described later in this section. However, the nature of output coupling in this TPG design drives an important requirement for the chip holder design. Because the 26° propagation angle of the THz waves within the crystal relative to the output facet is greater than the critical angle for total internal reflection at the LN-air interface (θ_{crit} = 11.5°), an intermediate output coupling medium is necessary. Prior work in LN-based TPG and TPO systems [35, 18] has shown that prisms made

of High-Resistivity Float Zone (HRFZ) silicon ($n_{THz} \approx 3.42$) are effective for output coupling of the THz waves.

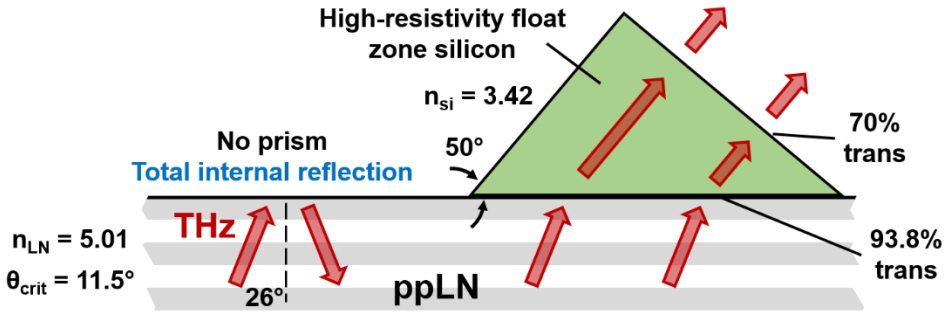

Figure 9 – A schematic showing the necessity of silicon prisms for output coupling to avoid total internal reflection of the THz waves within the ppLN crystal chip. The interface between the silicon and ppLN (prism base) is 10 mm long on each prism in the prototype system.

The prisms are designed to provide a smooth interface with the LN through proximity coupling, across which THz waves can propagate with some efficiency (93.8% transmission into the silicon and 70% into the air). To minimize internal reflection at the silicon-air interface (s-polarized output), the output facet of the silicon prism should be orthogonal to the THz propagation direction within the prism ($\theta_{Si} = 50°$ relative to the LN-silicon interface due to refraction). Because silicon exhibits moderate THz absorption ($\alpha \approx 0.2$ mm^{-1} at 1.5 THz), it is best to use multiple small prisms to minimize the THz propagation length within the silicon. Many small prisms would provide the most efficient output coupling, but this is limited by manufacturing constraints. In this work, we adopted the compromise used by several prior works [35, 18] that implements five prisms with "base" (LN-silicon interface) lengths of 10 mm, as shown in Figure 9. The chip holder was designed with a slot to accommodate proximity coupling of the silicon prisms to the output facet of the ppLN chip.

While THz generation is expected to be possible with an unseeded TPG system, as shown in the previous section, TPG efficiency is expected to scale with input seeding power in the signal (1070 nm) field. The requirements for an appropriate seeding source include polarized output (only the vertically-polarized component will participate in THz generation), relatively narrow bandwidth, and a sufficiently large output capacity to reach desired power levels. While there are many 1064 nm sources available based on Nd:YAG gain media, there are relatively few available at 1070 nm, and they are typically custom laser units. Ultimately, an option provided by Civil Laser (FLH-1070-30-SM) was chosen because of its high power (500 mW after accounting for the need for external polarization) and lower price that allowed it to fit within the constraints of the project budget. The laser has a fiber optic output that is collimated to a beam diameter of approximately 1 mm, consistent with the aperture of the TPG crystal. Characterization tests of the laser verified its wavelength tunability and power output. The results

of those tests are shown in Figure 10 and Figure 11 where wavelengths between 1070.0 nm and 1070.3 nm could be achieved by varying the TEC temperature set point between 45 °C and 75 °C.

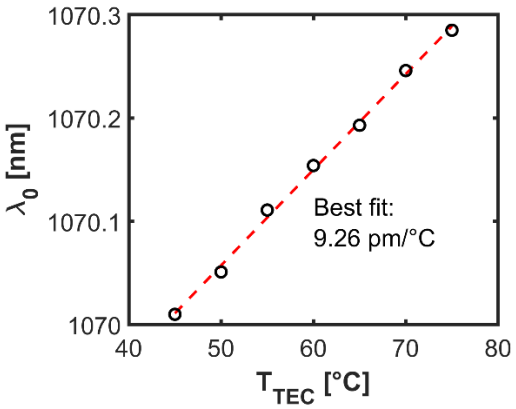

Figure 10 – Temperature tuning of the seeder laser output wavelength: 0.3 nm tuning range.

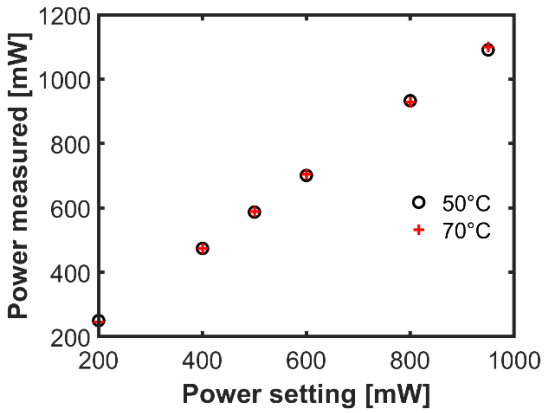

Figure 11 – Seeder laser power output compared to power setting on laser controller.

Verifying THz generation from the TPG system and understanding its spectral content will be important steps in characterizing the performance of this THz generation approach. To avoid the expense of a dedicated THz detector, we propose an indirect method based on near-IR spectroscopy to observe the THz generation process. Such a technique was demonstrated by Molter and co-workers [18, 37], whereby the spectrum of the near-IR beams transmitted from the TPG crystal was measured. Because the nonlinear wavelength conversion process is parametric, any increase in energy observed in the seeded 1070 nm signal field during the pump pulse (or signal generation in unseeded operation) necessarily implies THz generation at 1.49 THz.

Because relative changes in the seeded field can be difficult to measure accurately, observing cascaded generation processes can be a more sensitive approach to detecting THz generation. Cascaded processes occur when the generated THz field induces further downconversion of the signal field and upconversion of the pump field. These processes can cascade to even higher orders of downconversion, and Molter et al. reported observing up to third order downconversion as well as first order upconversion of the pump field [18]. Figure 12 shows an expected transmitted near-IR spectrum based on measurements reported by Molter et al., including a peak associated with Raman scattering from polariton modes in the crystal. As indicated, observation of the first order THz-induced pump upconversion and signal downconversion provides sensitive detection of THz generation. The drawback of this approach is that the cascaded processes cannot be expected to scale linearly with generated THz power, so it is not a precise

measurement of THz output power. However, the measured spectra can also be used to approximately gauge the generated THz wave's spectral bandwidth.

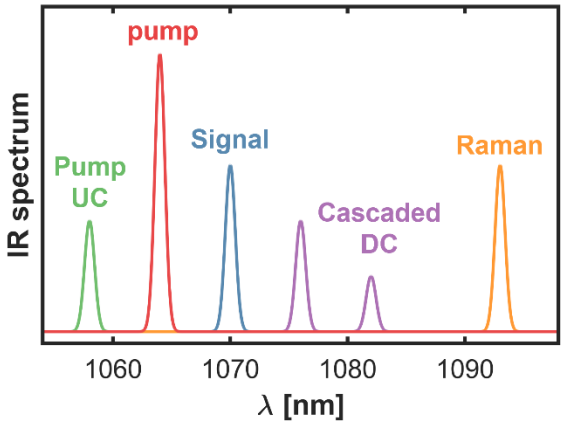

Figure 12 – A notional representation of the near-IR spectrum expected to be measured when testing the TPG system. The presence of pump UpConversion (UC) and cascaded DownConversion (DC) components would provide evidence of THz generation.

THz UCI detection module design

The design of the THz UCI module involves several design decisions that determine the system's capabilities and performance. The primary design decisions are the coordinated choice of the nonlinear crystal medium for upconversion and the wavelength of the laser pump beam. The desire to leverage available capital equipment, namely the Nd:YAG pulse-burst laser and high-speed silicon CMOS cameras, restricted the available pump wavelength choices to 532 nm and 1064 nm. While the option to use 1064 nm pumping would improve image quality, it would produce the upconverted image at near IR wavelengths. The silicon CMOS cameras used in this system exhibit much lower detection efficiency at those near IR wavelengths compared to their efficiency at visible wavelengths. The system in this work was designed to operate with 532 nm pumping to take advantage of the stronger camera response to maximize Signal-to-Noise Ratios (SNRs) in characterization measurements.

This choice of 532 nm pumping significantly restricts options for nonlinear crystal materials to host the SFG process because many are opaque for wavelengths below 600 nm. LN is the only candidate discussed in the previous section compatible with this pump wavelength. For this reason, the system is designed to perform SFG with QPM in ppLN chips. In addition to high-speed compatibility, this approach offers precision control over the system's spectral response through the choice of poling periods that determine the QPM condition.

As described in the previous section, the need to operate within "water windows" in the atmospheric THz transmission spectrum drives the selection of target THz frequencies. The choice of which water windows to hit must also consider how THz frequency affects image quality and THz absorption within the ppLN crystal. These are competing concerns as increasing THz frequencies will improve image quality (in terms of diffraction limited resolution) but will increase THz absorption within the ppLN crystal, which is undesirable. Therefore, we decided to target the highest THz frequency water windows below 1.6 THz to restrict the choices to those with acceptable absorption within the crystal and provide sub-millimeter scale spatial resolution. The choice of target THz frequencies directly informs the design of the ppLN crystal, as the poling period required for each THz frequency can be determined from Eq. (3). The chosen water window frequencies, as identified by Yang et al. [28], and the corresponding poling periods are given in Table 1. These poling periods were calculated assuming a crystal operating temperature of 100 °C.

Table 1 – List of THz frequencies targeted by the prototype THz UCI system and the corresponding poling periods required in the ppLN chip.

THz frequency	THz wavelength	Poling period in ppLN
0.68 THz	441 µm	171 µm
0.85 THz	353 µm	136 µm
1.35 THz	222 µm	84 µm
1.49 THz	201 µm	76 µm

As discussed previously, multiple poling periods can be fabricated on a single ppLN chip. The chip designed here contains the four poling periods side-by-side in the chip, each with 1 mm aperture widths. The aperture of the crystal was limited by the 1 mm thickness of the ppLN crystal, which was chosen to avoid high manufacturing costs. The total width of the chip is slightly greater than 5 mm to host the four poling periods. The length of the crystal chip along the direction of light propagation would typically be made as large as possible to increase the conversion efficiency, as shown in Eq. (4). However, due to THz absorption in ppLN, there are diminishing returns to increasing crystal length, as shown in Figure 2. Therefore, a propagation dimension length of 5 mm was chosen for the ppLN crystal in this work.

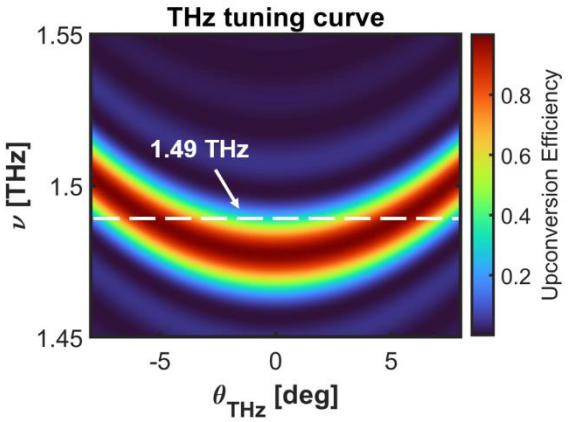

Figure 13 – THz tuning curve for the prototype UCI system design. Curve was computed assuming ppLN at 100 °C and a poling period of 76 µm. Target THz frequency of 1.49 THz is indicated by the dashed white line.

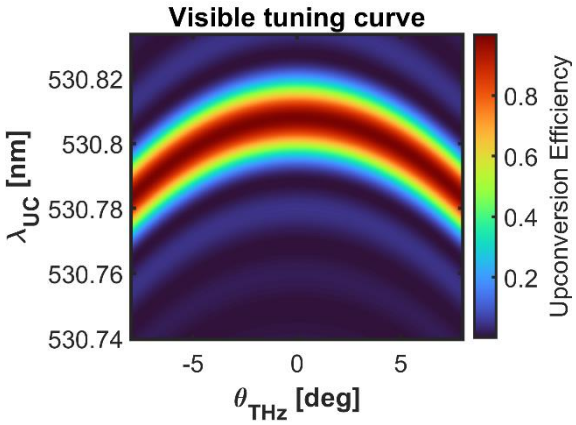

Figure 14 – Corresponding visible wavelength tuning curve. This shows the response of the UCI in terms of the upconverted spectrum generated by the system in response to uniform spectral illumination.

Like the ppLN chip used for THz generation, the crystal for UCI detection needs a custom mount designed to fit specific requirements. Specifically, the chip holder needs to act as an oven that maintains the temperature of the crystal at its design temperature, which is 100 °C for this system. The reasons for choosing a design temperature above room temperature are that it provides room for bidirectional temperature tuning, and the crystal is less susceptible to photorefractive damage from strong laser pumping at elevated temperatures. The UCI chip holder is machined from C100 copper and includes a socket for a ¼-inch cartridge heater that a PID controller can drive to maintain the crystal temperature. The crystal mounting surface of the holder is 10 mm × 10 mm, larger than required for the 5 mm × 5 mm footprint of the crystal in the current work. The larger mounting area will be able to accommodate other standard-sized ppLN chips that might be used for other applications, such as mid-IR UCI.

The upconverted image is formed using a 4f imaging configuration with a THz objective lens and a visible light image-forming lens. The objective lens is a 50 mm focal length PTFE lens placed at its focal length away from the object plane and the UCI crystal chip. The THz light carrying the target image and the 532 nm pump beam are combined with a piece of high conductivity ITO glass. The ITO glass reflects the THz light while efficiently transmitting the pump beam along the axis of the crystal. On the output side of the crystal, after the residual pump energy is rejected as described above, a 150 mm focal length N-BK7 lens forms the upconverted image focused on the detector of a high-speed silicon CMOS camera. By syncing

the high-speed camera's exposure with the pulse of the pump laser, a THz UCI measurement is captured for every pulse of the laser.

By design, the pump beam is significantly more energetic than the upconversion image signal generated through the upconversion process. Failure to effectively remove the pump beam energy from the imaging system would saturate the detector and prevent detection of the upconverted image. Partial rejection of the pump beam would create increased noise from the residual pump energy that would substantially reduce the measurement SNR. This motivates aggressive filtering of the pump beam, but accomplishing this goal is difficult because of the small spectral separation between the pump and upconverted wavelengths ($\lambda_{pump} \approx 532.2$ nm and $\lambda_{UC} \approx 530.8$ nm). In the prior example of THz UCI demonstrated by Tekavec et al. [14], reflective long-pass filters were used to separate the pump beam at 1064 nm from the UC signal (in that case, downconversion of the pump field was detected) at 1069.5 nm. While that wavelength shift can be accommodated with sharp optical filters, no optical filters can provide the fast cut-off required by the 532 nm pumped system in this work. Instead, alternative pump beam filtering approaches needed to be considered.

Several experimental studies related to THz upconversion detection have employed a combined filtering approach to rejecting pump energy [16, 38, 39]. This approach first rejects most of the pump power using very narrowband Volume Bragg Grating (VBG) filters that can achieve sub-nanometer width stop-bands. Following the VBG filters, one or more diffraction gratings act as dispersive elements that spatially separate the residual pump beam from the upconverted image. Application of the diffraction gratings leverages the narrowband nature of the upconverted image produced by the narrowband UCI response and THz source. The narrow bandwidth of the signal produces negligible dispersion broadening of the image, while the dispersion can be made sufficiently large to direct the pump beam outside the UCI field of view, where it can be blocked. This design uses two 2400 lines per mm holographic gratings to spatially filter the residual pump beam after two OD=4 VBG 532 nm notch filters.

One important consequence of using 532 nm SFG pumping and 1 mm aperture ppLN chips is that the THz UCI system will exhibit relatively poor spatial resolution. The poor image quality is due to the combined effects of upconversion de-magnification and spatial filtering by the limited crystal aperture. This design compromise was made to prioritize maximizing SNR in the prototype system to increase the likelihood that usable measurements could be acquired. The system design can be modified to improve image quality for future applications of THz UCI systems. These modifications are discussed in the suggested directions for future work in the next section. The feasibility of diffraction-limited THz UCI has already been demonstrated by Fan et al. [15] and Tekavec et al. [14]. Measurements with the prototype system designed in this work are intended to provide observations of system response that can determine if these

improvements to imaging quality can be practically implemented in high-speed THz UCI systems.

System integration and testing

With both sub-systems designed and developed, the final step is their integration into the complete prototype system layout. Figure 15 shows a schematic of the expected system layout, including all optical components. Using a single laser to pump both the THz generation and UCI detection eliminates the need for sophisticated timing coordination of the two pump beams. While the path length from the laser to the TPG module and then to the UCI module is slightly shorter than the path length for the UCI pump beam, the difference will not be important for the ~10 ns pulse durations.

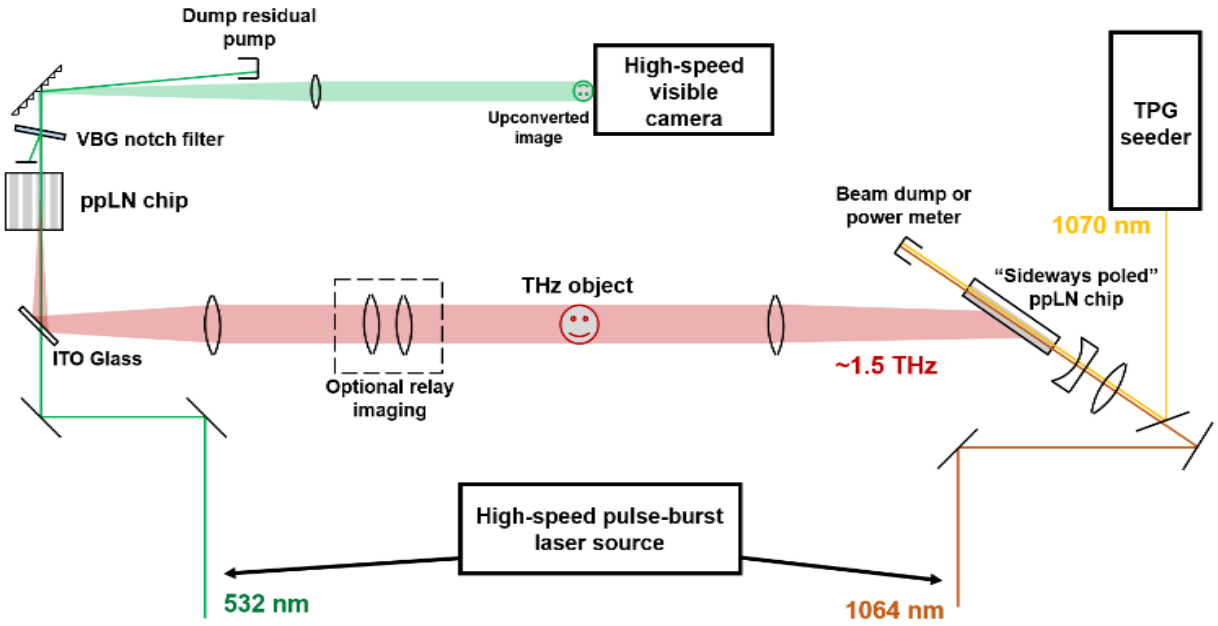

Figure 15 – Notional schematic of the prototype high-rate THz UCI system layout.

The purpose of the prototype high-speed THz UCI system is to evaluate the practicality of the approach and what performance might be expected from such a system. The system's performance can be primarily broken down into the system's detection efficiency, or response, and the system's spatial resolution. A key aspect of system testing to verify is that it can achieve high frame rates. However, the system can be operated at lower repetition rates, and its performance is expected to be unchanged. For this reason, most characterization tests can be performed at a low repetition rate before being scaled up to high speed at the same pulse

energies. The following proposed tests can be performed with pumping from a low-speed (10 Hz) Nd:YAG laser:

- Measure the response of the system to changing UCI pump energy to confirm linear scaling
- Measure the SNR of measurements from the UCI system at various intensities from the maximum TPG output to the minimum detectable level
- Estimate the Modulation Transfer Function (MTF) and Point-Spread Function (PSF) of the imaging system using a ruled calibration target
- Observe the variation in collected UCI intensity with crystal temperature to estimate the temperature tuning rate and capacity of the system

The final step of characterization would be to perform tests of the system at high rates using the pulse-burst laser system. The target repetition rate for these measurements would be 10k FPS. Successful tests at the target rate could motivate tests at up to 100k FPS to determine if the system can be used for applications with the fastest dynamics, such as explosions. Rapidly moving mechanical masks, such as a patterned flywheel like that used by Downes et al. [13], could be used to verify frame rates. Some low-speed tests related to the system's response efficiency and SNR may need to be repeated to verify no performance loss at high speeds. Other performance aspects, such as the system's imaging resolution and temperature tuning, are unlikely to change with pulse rate and would not need to be tested. The data from these tests could be used to assess the practical capabilities and limits of high-speed THz UCI and to design high-performance UCI systems for applications of interest.

ANTICIPATED OUTCOMES AND IMPACTS

The impacts of this project comprise gains in both material assets and personnel expertise. The material gains include developing a feasible high-speed THz UCI system design and procuring the necessary materials to implement it at the labs. This project has produced significant institutional knowledge and experience in THz generation, detection, and UCI. This report contains an overview of the prototype system design and the analysis methodology that led to it.

The primary outcome of this project is the generation of the high-speed THz UCI prototype system design. This system, currently in assembly and testing, is expected to produce the highest THz imaging frame rates ever demonstrated. This prototype system can produce data that can be used to develop application-ready versions of high-speed THz imaging systems. Through the use of this prototype system platform, Sandia will be able to establish itself as a leader in the development of THz imaging technologies. The system can be modified at a relatively low cost to improve imaging quality or test different UCI approaches. In this way, we see the high-speed THz UCI system as an asset that can provide dividends beyond this project's scope.

In addition, the THz generation sub-system of the THz UCI prototype can itself be an asset for future THz work at Sandia. The nature of THz UCI placed specific requirements on the THz source for active imaging. The TPG approach adopted in this work is expected to provide high-energy THz pulses at high rates (up to and above 100 kHz). This high-rate source is an important capability that can be applied beyond the UCI system. While it does not produce the broadband THz radiation typically used for time-domain spectroscopy, it can still be used for pointwise extinction and reflection measurements.

Continuing work

All near-term follow-on work related to this project would be focused on testing and characterizing the prototype UCI system. The specific tests and data to be collected are described at the end of the previous section. Further tests might also be performed to better characterize the system if support for them is available. For example, if we gained access to a calibrated THz power meter, then the pulse energy output from the TPG system could be reliably quantified. This would, in turn, allow for measurement of the Noise-Equivalent Power (NEP) of the THz UCI system, an important metric for characterizing detector sensitivity.

The design and testing of this prototype high-speed THz UCI system are anticipated to be reported in a future journal publication. The system will achieve the highest frame rate of any THz imaging system and represent a breakthrough for applied THz imaging. This will be of interest to the broader scientific community, both in terms of the approach taken and the performance results of the high-speed measurements. In addition, future conference attendance would increase the visibility of this work in the optics community and potentially open up opportunities for collaborations.

Recommendations for future work

The design process and preliminary testing have identified several avenues for future work. Some of these were planned as part of the prototype approach, while others are the results of lessons learned throughout the project. The planned improvements to take the system from prototype status to application-ready focus on modifications to the UCI module that will enhance image quality. Design and development of the QPM-based THz generation revealed opportunities for improvement of that sub-system.

The pump wavelength of the UCI process was chosen to be 532 nm to maximize SNR of detection for characterization measurements. However, this choice compromised the image quality that the prototype system can produce because of the significant UCI de-magnification that results from shorter wavelength pumping. Modifying the system to operate with 1064 nm

pumping will improve image quality by reducing UCI de-magnification by a factor of two. Imaging measurements by Tekavec et al. [14] showed that imaging at 1.5 THz using 1064 nm can achieve millimeter-scale imaging resolution. Imaging with this quality could be realized with a high-speed system using 1064 nm pumping from a pulse-burst Nd:YAG.

Another modification that could improve the imaging quality of the UCI system would be to increase the aperture of the nonlinear crystal. Because the SFG process acts like a spatial aperture at the Fourier plane of the 4f imaging system, the diameter of the pump beam performs spatial filtering of the upconverted image. The spatial resolution that can be achieved with the system will be improved by increasing the diameter of the pump beam. However, in this system, the pump beam diameter is limited to 1 mm by the aperture of the crystal. The thickness of the ppLN chip, the limiting dimension due to the periodic poling process, can be increased to about 2 mm with available manufacturing capabilities. However, this would increase the cost of the ppLN chip, and apertures larger than 2 mm are not currently available with ppLN. To enjoy the largest possible apertures requires consideration of other nonlinear crystal materials.

Prior low-speed THz UCI works have demonstrated GaAs [14] and DAST [15] crystals as effective for imaging. Other nonlinear crystal candidates that might be explored include OP-GaP and OH1. The advantage of these crystals is that they can be fabricated with larger apertures than ppLN chips. Additionally, these alternative crystal materials typically have lower THz absorption coefficients than LN. Depending on the effective nonlinear coefficient of the material, this could lead to improved SFG conversion efficiencies. That absorption reduction would offset some of the SNR reduction associated with a change to 1064 nm pumping.

With respect to the THz generation system, the orthogonal QPM approach provides a high-energy pulsed approach that can feasibly scale to high repetition rates. However, subsequent analysis and discussions with experienced practitioners [37] have identified potential improvements for this generation strategy. With the exactly 90 degree poling period adopted in this work, the THz propagation direction becomes degenerate with equal THz power propagating to the right and left of the pump beam axis. This effectively halves the THz generation efficiency, as only the component of THz light propagation toward the output facet will leave the crystal before being absorbed. An alternative slant-stripe approach, where the poling period is inclined at an angle near to 90 degrees, is described by Molter [18]. This approach will only generate THz radiation in one direction when operated with signal beam seeding. In this way, the THz generation efficiency would be improved by approximately a factor of 2. Additionally, having the domain boundaries in the poled region be non-parallel to the pump beam is expected to improve beam quality and damage threshold. Molter demonstrated a poling slant angle of 84 degrees relative to the pump beam [37].

Potential applications

In addition to completing the characterization tests with the prototype system, it could be tested in specific applications after making the modifications discussed above. One area where active THz imaging could be immediately applied is studies of dense, aerosolized sprays. These are regularly studied in the context of gasoline and diesel fuel direct injection technologies where regions of the sprays near the injector are very optically dense. Almost complete extinction occurs at visible wavelengths, so quantitative extinction becomes infeasible in the near-injector regions. The Mie scattering cross-section of the fuel droplets scales inversely with the illumination wavelength. In this way, THz imaging can be used to perform imaging extinction measurements through these dense sprays.

An additional application to explore is imaging in explosion and impact environments. In explosions dust, soot, and other fine debris obscure imaging measurements in regions within the outer shockwave. THz illumination would mitigate scattering from these small particles in the same way that scattering from droplets is reduced. THz imaging might enable imaging of wave structures and dynamics within regions of the explosions and impacts that are opaque to visible light. The ns pulse durations of the THz source in this work would effectively freeze the fast dynamics of these environments. The THz UCI system can theoretically be scaled to MHz frame rates that could be capable of observing dynamics and increasing data throughput from these expensive experiments. Exploration of this field of applications could be fruitful.

CONCLUSION

This project explored approaches to enabling high-rate THz imaging through UCI-based techniques. The study produced a design for a prototype high-speed THz UCI system that can investigate the practical capabilities and limitations of the THz UCI method. All necessary materials for the prototype system have been procured, and assembly and initial characterization tests of the system have begun. This system provides a platform that can be used to develop high-speed THz imaging solutions that can be applied to support Sandia's missions.

Some of the key findings that have resulted from this research and design effort include:

- Despite strong THz absorption, ppLN crystal chips can be used to create wavelength-flexible THz UCI systems
- Commonly used broadband THz sources, such as PCAs and OR, are poor candidates for THz UCI systems because of the narrowband response of THz UCI systems
- A sideways QPM TPG process in ppLN provides a high-energy, narrowband THz source that can scale to high repetition rates, satisfying the requirements of high-speed THz UCI
- The use of 532 nm SFG pumping along with aggressive filtering of residual pump energy in the imaging system will maximize the SNR of characterization measurements

Immediate continuations of this work on THz UCI would focus on completing characterization testing of the prototype system. The data collected from these measurements could be used to design high-speed THz UCI systems with improved performance, especially in terms of spatial resolution. Several avenues for future work are proposed in this report, including potential applications for high-rate THz imaging.

ACKNOWLEDGMENTS

The authors would like to thank François Leonard (08342) for his collaboration and help with understanding THz generation and detection. We would like to thank Daniel Molter for discussion and suggestions about THz generation and the sideways QPM TPG technique applied in this work. We would like to thank Vladimir Kozlov for discussions about THz UCI and THz generation. We thank Peter Schunemann for help with understanding nonlinear crystal options for THz generation. We thank James MacDonald (08361) for reviewing this report and providing helpful edits.

REFERENCES

[1] Jansen, C., Wietzke, S., Peters, O., Scheller, M., Vieweg, N., Salhi, M., Krumbholz, N., Jördens, C., Hochrein, T., & Koch, M. (2010). Terahertz imaging: applications and perspectives. *Applied Optics*, *49*(19), E48. https://doi.org/10.1364/ao.49.000e48

[2] Karpowicz, N., Zhong, H., Zhang, C., Lin, K.-I., Hwang, J.-S., Xu, J., & Zhang, X.-C. (2005). Compact continuous-wave subterahertz system for inspection applications. *Applied Physics Letters*, *86*(5), 054105. https://doi.org/10.1063/1.1856701

[3] Jördens, C., & Koch, M. (2008). Detection of foreign bodies in chocolate with pulsed terahertz spectroscopy. *Optical Engineering*, *47*(3), 037003. https://doi.org/10.1117/1.2896597

[4] Jördens, C., Scheller, M., Wietzke, S., Romeike, D., Jansen, C., Zentgraf, T., Wiesauer, K., Reisecker, V., & Koch, M. (2010). Terahertz spectroscopy to study the orientation of glass fibres in reinforced plastics. *Composites Science and Technology*, *70*(3), 472–477. https://doi.org/10.1016/j.compscitech.2009.11.022

[5] Hernandez-Cardoso, G. G., Rojas-Landeros, S. C., Alfaro-Gomez, M., Hernandez-Serrano, A. I., Salas-Gutierrez, I., Lemus-Bedolla, E., Castillo-Guzman, A. R., Lopez-Lemus, H. L.,

& Castro-Camus, E. (2017). Terahertz imaging for early screening of diabetic foot syndrome: A proof of concept. *Scientific Reports*, *7*(1). https://doi.org/10.1038/srep42124

[6] Leahy-Hoppa, M. R., Fitch, M. J., & Osiander, R. (2009). Terahertz spectroscopy techniques for explosives detection. *Analytical and Bioanalytical Chemistry*, *395*(2), 247–257. https://doi.org/10.1007/s00216-009-2803-z

[7] Linne, M. A., Paciaroni, M., Berrocal, E., & Sedarsky, D. (2009). Ballistic imaging of liquid breakup processes in dense sprays. *Proceedings of the Combustion Institute*, *32*(2), 2147–2161. https://doi.org/10.1016/j.proci.2008.07.040

[8] Maes, N., Dam, N., Somers, B., Lucchini, T., D'Errico, G., & Hardy, G. (2016). Experimental and Numerical Analyses of Liquid and Spray Penetration under Heavy-Duty Diesel Engine Conditions. *SAE International Journal of Fuels and Lubricants*, *9*(1), 108–124. https://doi.org/10.4271/2016-01-0861

[9] McNesby, K. L., Homan, B. E., Benjamin, R. A., Boyle, V. M., Densmore, J. M., & Biss, M. M. (2016). Invited Article: Quantitative imaging of explosions with high-speed cameras. *Review of Scientific Instruments*, *87*(5), 051301. https://doi.org/10.1063/1.4949520

[10] Neu, J., & Schmuttenmaer, C. A. (2018). Tutorial: An introduction to terahertz time domain spectroscopy (THz-TDS). *Journal of Applied Physics*, *124*(23), 231101. https://doi.org/10.1063/1.5047659

[11] "GMP Inc.," [Online]. Available: https://www.gmp.ch/laser-measurement-modulation/thz-measurement-detectors/uncooled-real-time-thz-imager-rigi-camera.

[12] "DataRay Inc.," Available: https://dataray.com/collections/all/products/wincamd-thz-usb-3-0-1-cmos-thz-beam-profiler-system.

[13] Downes, L. A., MacKellar, A. R., Whiting, D. J., Bourgenot, C., Adams, C. S., & Weatherill, K. J. (2020). Full-Field Terahertz Imaging at Kilohertz Frame Rates Using Atomic Vapor. *Physical Review X*, *10*(1). https://doi.org/10.1103/physrevx.10.011027

[14] Tekavec, P. F., Kozlov, V. G., McNee, I., Spektor, I. E., & Lebedev, S. P. (2015). Video rate imaging of narrow band THz radiation based on frequency upconversion. In L. P. Sadwick & T. Yang (Eds.), *SPIE Proceedings*. SPIE. https://doi.org/10.1117/12.2080379

[15] Fan, S., Qi, F., Notake, T., Nawata, K., Takida, Y., Matsukawa, T., & Minamide, H. (2015). Diffraction-limited real-time terahertz imaging by optical frequency up-conversion in a DAST crystal. *Optics Express*, *23*(6), 7611. https://doi.org/10.1364/oe.23.007611

[16] Pfeiffer, T., Kutas, M., Haase, B., Molter, D., & von Freymann, G. (2020). Terahertz detection by upconversion to the near-infrared using picosecond pulses. *Optics Express*, *28*(20), 29419. https://doi.org/10.1364/oe.397839

[17] Kawase, K., ichi Jun-Shikata, Imai, K., & Ito, H. (2001). Transform-limited, narrow-linewidth, terahertz-wave parametric generator. *Applied Physics Letters*, *78*(19), 2819–2821. https://doi.org/10.1063/1.1370988

[18] Molter, D., Theuer, M., & Beigang, R. (2009). Nanosecond terahertz optical parametric oscillator with a novel quasi phase matching scheme in lithium niobate. *Optics Express*, *17*(8), 6623. https://doi.org/10.1364/oe.17.006623

[19] Barh, A., Tawfieq, M., Sumpf, B., Pedersen, C., & Tidemand-Lichtenberg, P. (2019). Upconversion spectral response tailoring using fanout QPM structures. *Optics Letters*, *44*(11), 2847. https://doi.org/10.1364/ol.44.002847

[20] Huang, K., Fang, J., Yan, M., Wu, E., & Zeng, H. (2022). Wide-field mid-infrared single-photon upconversion imaging. *Nature Communications*, *13*(1). https://doi.org/10.1038/s41467-022-28716-8

[21] Fejer, M. M., Magel, G. A., Jundt, D. H., & Byer, R. L. (1992). Quasi-phase-matched second harmonic generation: tuning and tolerances. *IEEE Journal of Quantum Electronics*, *28*(11), 2631–2654. https://doi.org/10.1109/3.161322

[22] Schunemann, P. G., Pomeranz, L. A., & Magarrell, D. J. (2015). Optical parametric oscillation in quasi-phase-matched GaP. In K. L. Vodopyanov (Ed.), *SPIE Proceedings*. SPIE. https://doi.org/10.1117/12.2080821

[23] Sutherland, R. L., McLean, D. G., Kirkpatrick, S. (2003). Handbook of Nonlinear Optics. Marcel Dekker.

[24] Maestre, H., Torregrosa, A. J., Fernández-Pousa, C. R., & Capmany, J. (2018). IR-to-visible image upconverter under nonlinear crystal thermal gradient operation. *Optics Express*, *26*(2), 1133. https://doi.org/10.1364/oe.26.001133

[25] White, L. (2020). Pulsed Mid-Infrared Upconversion Imaging in Rotating Detonation Engines. University of Michigan. Dissertation.

[26] Barh, A., Rodrigo, P. J., Meng, L., Pedersen, C., & Tidemand-Lichtenberg, P. (2019). Parametric upconversion imaging and its applications. *Advances in Optics and Photonics*, *11*(4), 952. https://doi.org/10.1364/aop.11.000952

[27] Jazbinsek, M., Puc, U., Abina, A., & Zidansek, A. (2019). Organic Crystals for THz Photonics. *Applied Sciences*, *9*(5), 882. https://doi.org/10.3390/app9050882

[28] Yang, Y., Shutler, A., & Grischkowsky, D. (2011). Measurement of the transmission of the atmosphere from 02 to 2 THz. *Optics Express*, *19*(9), 8830. https://doi.org/10.1364/oe.19.008830

[29] Burford, N. M., & El-Shenawee, M. O. (2017). Review of terahertz photoconductive antenna technology. *Optical Engineering*, *56*(1), 010901. https://doi.org/10.1117/1.oe.56.1.010901

[30] Faure, J., Tilborg, J. V., Kaindl, R. A., & Leemans, W. P. (2004). Modelling Laser-Based Table-Top THz Sources: Optical Rectification, Propagation and Electro-Optic Sampling. *Optical and Quantum Electronics*, *36*(8), 681–697. https://doi.org/10.1023/b:oqel.0000039617.85129.c2

[31] Tekavec, P. F., & Kozlov, V. G. (2014). High power THz sources for nonlinear imaging. *AIP Conference Proceedings*. https://doi.org/10.1063/1.4865011

[32] Stothard, D. J. M., Edwards, T. J., Walsh, D., Thomson, C. L., Rae, C. F., Dunn, M. H., & Browne, P. G. (2008). Line-narrowed, compact, and coherent source of widely tunable terahertz radiation. *Applied Physics Letters*, *92*(14), 141105. https://doi.org/10.1063/1.2907489

[33] Walsh, D., Stothard, D. J. M., Edwards, T. J., Browne, P. G., Rae, C. F., & Dunn, M. H. (2009). Injection-seeded intracavity terahertz optical parametric oscillator. *Journal of the Optical Society of America B*, *26*(6), 1196. https://doi.org/10.1364/josab.26.001196

[34] Yarborough, J. M., Sussman, S. S., Purhoff, H. E., Pantell, R. H., & Johnson, B. C. (1969). Efficient, tunable optical emission from $LiNbO_3$ without a resonator. *Applied Physics Letters*, *15*(3), 102–105. https://doi.org/10.1063/1.1652910

[35] Kawase, K., Minamide, H., Imai, K., ichi Jun-Shikata, & Ito, H. (2002). Injection-seeded terahertz-wave parametric generator with wide tunability. *Applied Physics Letters*, *80*(2), 195–197. https://doi.org/10.1063/1.1429299

[36] Nawata, K., Tokizane, Y., Takida, Y., & Minamide, H. (2019). Tunable Backward Terahertz-wave Parametric Oscillation. *Scientific Reports*, *9*(1). https://doi.org/10.1038/s41598-018-37068-7

[37] Molter, D. (2010). Novel approaches in coherent terahertz measurement techniques. Technical University of Kaiserslautern. Dissertation.

[38] Kutas, M., Haase, B., Klier, J., Molter, D., & von Freymann, G. (2021). Quantum-inspired terahertz spectroscopy with visible photons. *Optica*, *8*(4), 438. https://doi.org/10.1364/optica.415627

[39] Haase, B., Kutas, M., Riexinger, F., Bickert, P., Keil, A., Molter, D., Bortz, M., & von Freymann, G. (2019). Spontaneous parametric down-conversion of photons at 660 nm to the terahertz and sub-terahertz frequency range. *Optics Express*, *27*(5), 7458. https://doi.org/10.1364/oe.27.007458

ADDENDUM

LABORATORY DIRECTED
RESEARCH & DEVELOPMENT
WHERE INNOVATION BEGINS

TPG chip holder drawing

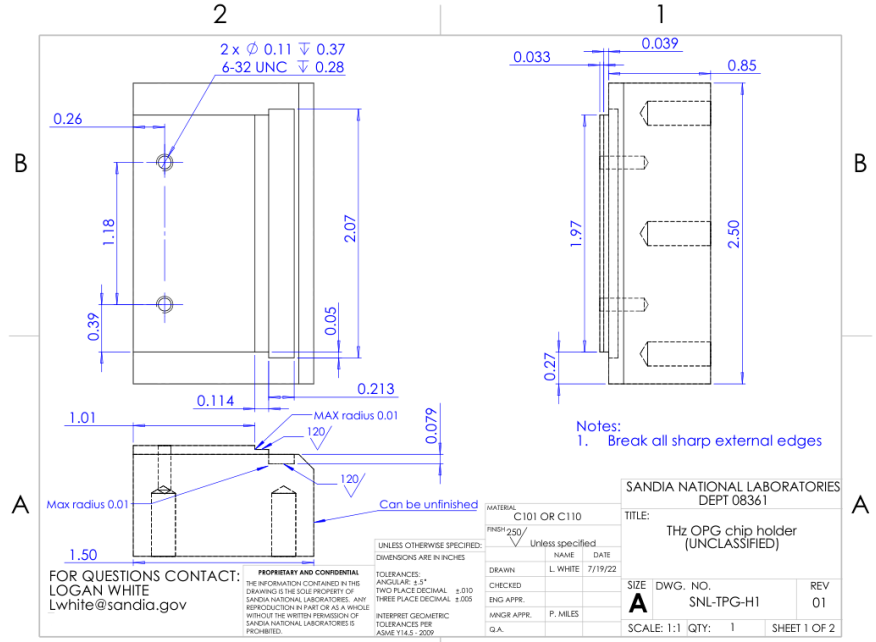

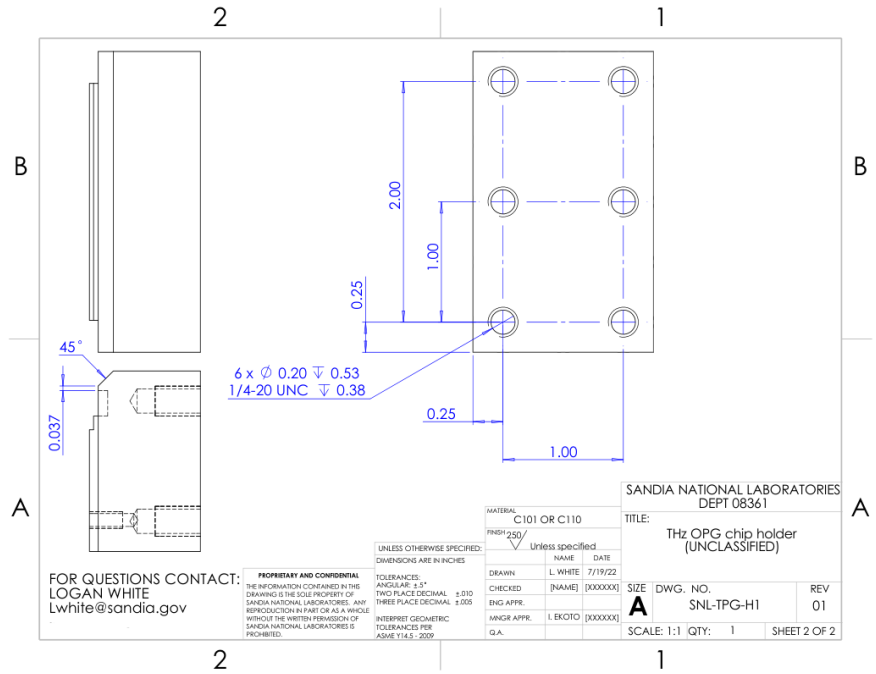

LABORATORY DIRECTED
RESEARCH & DEVELOPMENT
WHERE INNOVATION BEGINS

UCI chip holder drawing